Special Issue of the 6th International Congress & Exhibition (APMAS2016), Maslak, Istanbul, Turkey, June 1–3, 2016

Investigation of Mechanical Properties of Fe-Based Metal Matrix Composites by Warm Compaction for Gear Production

T. Gun[a,*] and M. Simsir[b]

[a]ESTAŞ Eksantrik San. ve Tic. A.Ş. Sivas, Turke, 58060, Sivas, Turkey

[b]Cumhuriyet University Department of Metallurgical and Materials Engineering, 58140, Sivas, Turkey

In this study, mechanical behavior of iron-based (Fe-0.8C-2.0Cu-4.5Ni-1.8Mo-1.0B (wt.%)) metal matrix composite synthesized by powder metallurgy was investigated for gear production. Metal matrix composite has been produced by warm compaction, followed by free sintering in controlled Ar gas atmosphere. Green composite was produced under pressure of 650 MPa at 160 °C. The green products have been sintered at various temperatures (1050, 1150 and 1250 °C) and for various time periods (30, 60 and 90 min). Mechanical tests (hardness and wear tests) have been conducted. The microstructure and the worn surfaces of the samples have been examined under scanning electron microscope and analyzed by energy dispersive spectroscopy and X-ray diffraction method. The results have shown that hardness and wear resistance of the samples increase with increasing sintering temperature and time. Effect of sintering temperature is greater than that of sintering time. The highest hardness and wear resistance have been obtained in the composite sample produced at 1250 °C for 90 min.

DOI: 10.12693/APhysPolA.131.443

PACS/topics: 81.20.ev, 87.15.La, 87,64.M

1. Introduction

Powder metallurgy (PM) technique is experiencing growth and is replacing traditional metal-forming operations because of its low relative energy consumption, high material utilization, and low capital cost [1]. Therefore some PM steels with high sintered density as well as high wear resistance have found wide application in the automotive industry, in engine and transmission systems, mainly for wear loaded components, such as cam lobes etc. [2].

Fe-Cu and Fe-Cu-C based PM parts are important for the industry. These parts are used in many applications that require high strength, hardness and wear resistance. Fe-based materials produced by powder metallurgy methods are used in camshafts, connecting rods, sprockets, pulleys, various valves, clutch adjustment rings, arm turbine converters, oil pump gears and many applications in the automotive industry [3].

For parts formed with the cold-pressing process of powder metallurgy, different sintering methods are used, free sintering, hot press sintering, hot isostatic sintering, spark plasma sintering, microwave sintering etc. In this study, the warm compaction method was used for production of metal matrix composites. This technique consists in pressing a pre-heated powder in a heated die at a temperature typically ranging from 90 to 150 °C. The green strength obtained from this approach is about two times larger than that provided by cold compaction [4–9]. By heating the powder mix and the press tool to 150 °C an increase in density in the range of 0.15–0.20 g/cm^3 over conventional compaction was reported [10, 11].

The aim of this study is to produce Fe-based (Fe-0.8C-2.0Cu-4.5Ni-1.8Mo-1B (wt.%)) metal matrix composite by warm compacting method and to investigate the mechanical properties of produced metal matrix composite for gear production.

2. Materials and equipment

Water-atomized iron powder, together with nickel, copper, molybdenum, boron and graphite with purity higher than 99%, were used for this experiment. The average diameter of particles was in the range of <68 μm for iron, <44 μm for copper, <37 μm for nickel, <88 μm for molybdenum, <15 μm for boron powder and graphite powder. The composition of powder mixture is 0.8 wt.% C, 2 wt.% Cu, 4.5 wt.% Ni, 1.8 wt.% Mo, 1 wt.% B, 0.6 wt.% zinc stearate and iron base. The powder mixtures were homogenized in a TURBULA mixer for 30 min. The pre-heated mixed powders were pressed in a steel mold at temperature from room temperature to 160 °C. Compacting pressure was 650 MPa. Cylindrical specimens were obtained with the dimension of 15 × 10 mm. The pre-pressed compacts were sintered in argon atmosphere, at three different temperatures of 1050, 1150, 1250 °C and held for 30, 60 and 90 min in the sintering furnace for each temperature. The sintered specimens were tested to determine wear behavior, hardness, density and microstructure. SEM with EDS and XRD analyzes were conducted on the sintered specimens. The effects of the sintering temperature and time on material properties were investigated.

*corresponding author; e-mail: tarik.gun@estas.com.tr

3. Results and discussion

Hardness tests were conducted in the INSTRON-WOLPERT macro hardness tester. HRA hardness values of the specimens were measured using 60 kgf loads. Five hardness measurements were carried out for each sample and the mean of the hardness and density values are given in Table. The theoretical density of composite material of 7.8 g/cm^3 was calculated. The density of sintered compacts was measured using Archimedes principle and calculated using Eq. 1

$$\rho_{\text{exp}} = \rho_{\text{water}} \left(\frac{m_{\text{air}} - m_{\text{water}}}{m_{\text{air}}} \right). \quad (1)$$

Then, percentage of porosity was calculated according to following equation

$$\%\,\text{porosity} = \frac{\rho_{\text{th}} - \rho_{\text{exp}}}{\rho_{\text{th}}} \times 100. \quad (2)$$

TABLE I

Hardness and density measurement results.

T [°C]	Time [min.]	$\rho_{\text{experimental}}$ [g/cm^3]	Porosity [%]	HRa
1050	30	6.81	12.69	48.3
	60	6.85	12.18	49.7
	90	6.87	11.90	52.4
1150	30	6.93	11.15	53.7
	60	6.97	10.64	65.8
	90	7.00	10.25	68.4
1250	30	7.03	9.87	73.1
	60	7.08	9.23	74.8
	90	7.11	8.45	75.6

As it is seen, the hardness and the density values increase with increasing sintering temperature and time. The maximum hardness was obtained in the samples sintered at 1250 °C for 90 minutes. The amount of porosity seems to be decreasing with increasing sintering temperature and time. The maximum amount of porosity was obtained in the sintered sample at 1050 °C for 30 min.

Wear tests were carried out on Nanove "Ball-on-disc" wear measurement apparatus. The wear tests were carried out under load of 30 N, at 300 rpm speed and using sliding distances of 100 m.

Then the friction coefficient and weight loss were measured. Figure 1 shows the relationship between weight loss and friction coefficient for various sintering processes. The highest coefficient of friction was measured in the sample sintered at 1150 °C for 90 minutes. Minimum measured sample loss of 2.3 mg was the result of an increase in the surface hardness in sample sintered at 1250 °C for 90 minutes.

SEM analyzes were conducted to characterize the worn surface as a result of the wear test. Figure 2 shows the worn surfaces of the samples. At applied wear test conditions (30 N, at 300 rpm speed and sliding distances of 100 m), two wear mechanisms (adhesive and abrasive wear) are seen on the worn surfaces of the sintered

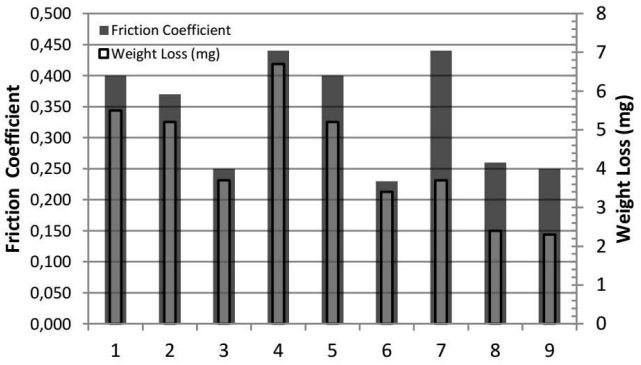

Fig. 1. Wear test results of samples sintered at 1050 °C (1) 30 min, (2) 60 min, (3) 90 min; at 1150 °C (4) 30 min, (5) 60 min, (6) 90 min; at 1250 °C (7) 30 min, (8) 60 min, (9) 90 min.

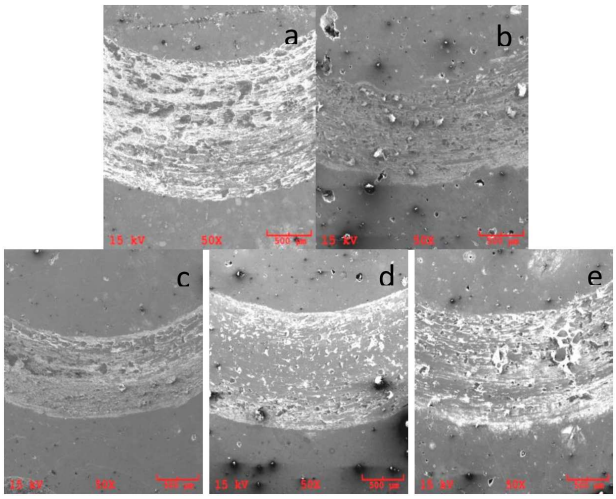

Fig. 2. Worn surfaces of samples sintered at (a) 1050 °C for 90 min; (b) 1150 °C for 90 min; (c) 1250 °C for 30 min; (d) 1250 °C for 60 min; (e) 1250 °C for 90 min.

samples. Mainly adhesive wear is seen in all samples, however there was also partial abrasive wear. Since the ball hardness had remained high compared to that of samples, that predominance of the adhesive wear is considered normal. The worn surface of the samples is characteristic of adhesive wear, which can be also supported by the coarsening of ball surface.

Cavities observed on the surfaces of three types of sintered samples are due to adhesive wear. Amount of cavities on the worn surface decreases as the sintering time increases (Fig. 2a, b and c). Similar situation was observed when the sintering temperature was decreased (Fig. 2c, d and e). As it is well known, the densification of sintered samples decreases, while sintering time and temperature decreases. Cavities on the surface are attributed to fact, that the contact interface between two surfaces resists to relative sliding. A large plastic deformation is introduced in the contact region under tangential shearing, due to compression load. Because of deformation in the contact region, a crack is initiated and is propagated in the

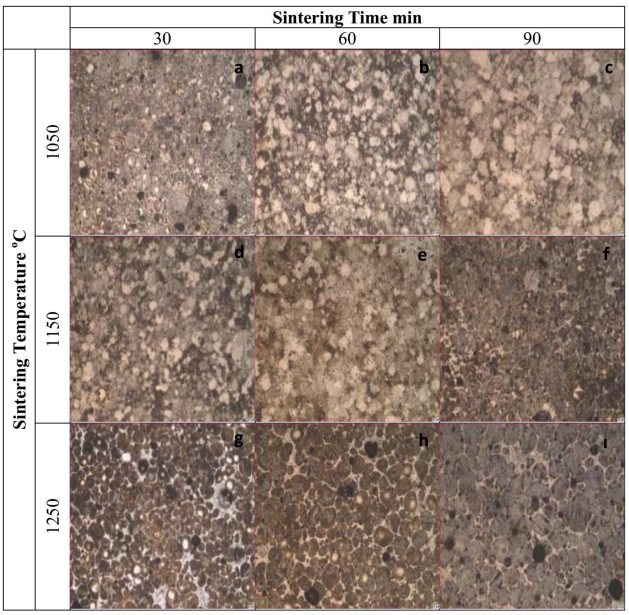

Fig. 3. The microstructure of samples at 1050 °C (a) 30 min, (b) 60 min, (c) 90 min; at 1150 °C (d) 30 min, (e) 60 min, (f) 90 min; at 1250 °C (g) 30 min, (h) 60 min, (i) 90 min.

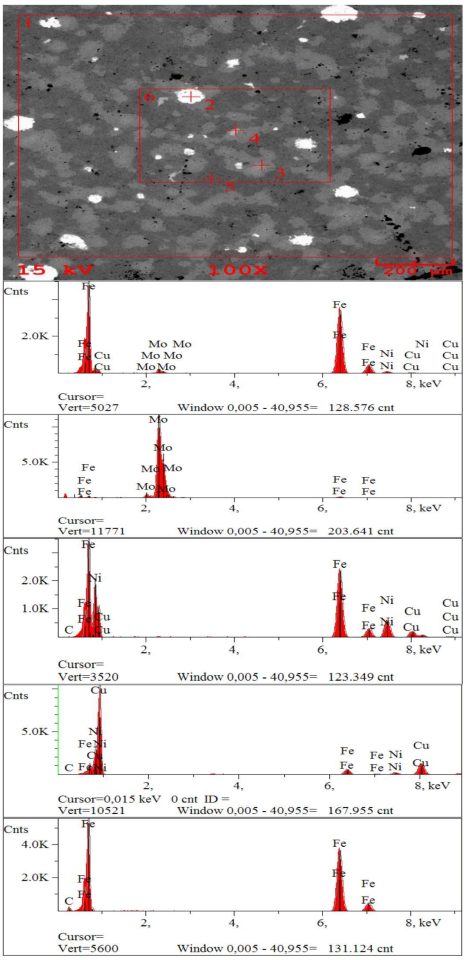

Fig. 4. SEM+EDX analysis of sample sintered at 1050 °C for 90 minutes.

combined fracture mode of tensile and shear loads. When the crack reaches the contact interface, a wear particle is separated from the surface and cavity on the surface is formed.

Although adhesive wear tests were performed, it was observed that wear mechanism has changed from adhesive to abrasive wear during the test. Grooves were observed on the worn surface for sintered samples due to abrasive wear (especially Fig. 2c). Grooves were formed as the result of wear particle generation during the test period. Another reason of groove formation is due to microcutting of the surface of the wearing material by the hard material (roller), since the harder material (roller) penetrates the softer one (material), and interlocking between surfaces is formed under compression load. Depth of the groove increases with decreasing surface hardness of the materials. The wear loss is proportional to the normal compression load, and it is inversely proportional to the hardness of the wearing material. In fact, abrasive wear resistance is linearly proportional to hardness of wearing materials. Plastic deformation was observed due to the plastic flow of material forming ridges on both sides of a groove.

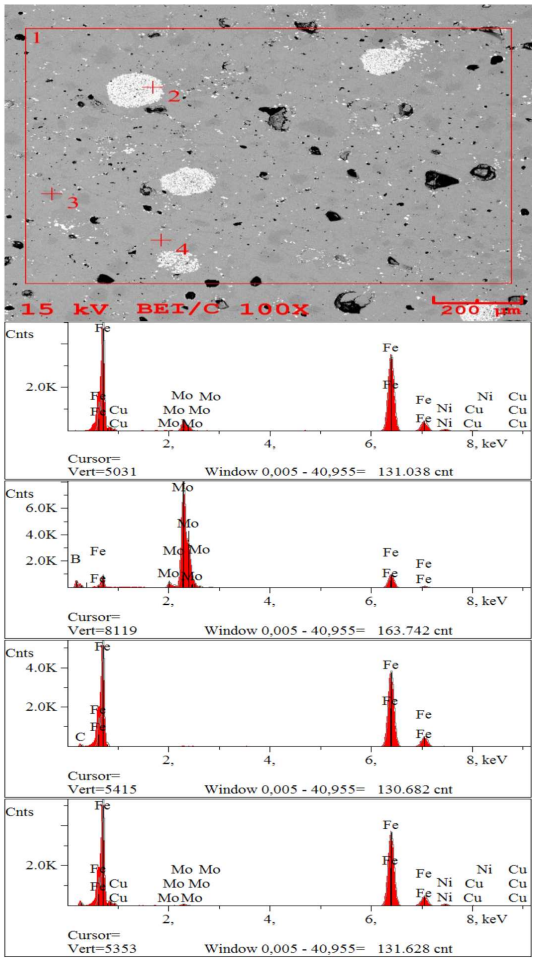

Fig. 5. SEM+EDX analysis of sample sintered at 1150 °C for 90 minutes.

Metallographic sections were prepared by grinding, diamond polishing, and etching in 2% Nital for 5–10 s. The metallographic observations were conducted on a metal microscope Nikon Eclipse MA200. Figure 3 shows the metallographic structure of the samples after Nital etching.

The microstructure of the sintered samples shows increase of copper solubility in the matrix and subsiding to the grain boundaries with the increasing sintering temperature and time. Mo and Cu addition have caused the formation of ferritic and regional bainitic microstructure. Changes in the ferrite grain shape and distribution has been observed with the increase of sintering temperature.

Figure 3 shows that there is an influence of the starting particle size on the austenite grain size. Increasing the sintering time to 1050 °C has resulted in austenite grains, which have approximately doubled in size. However the austenite grains were found to change phase with the increasing sintering temperature.

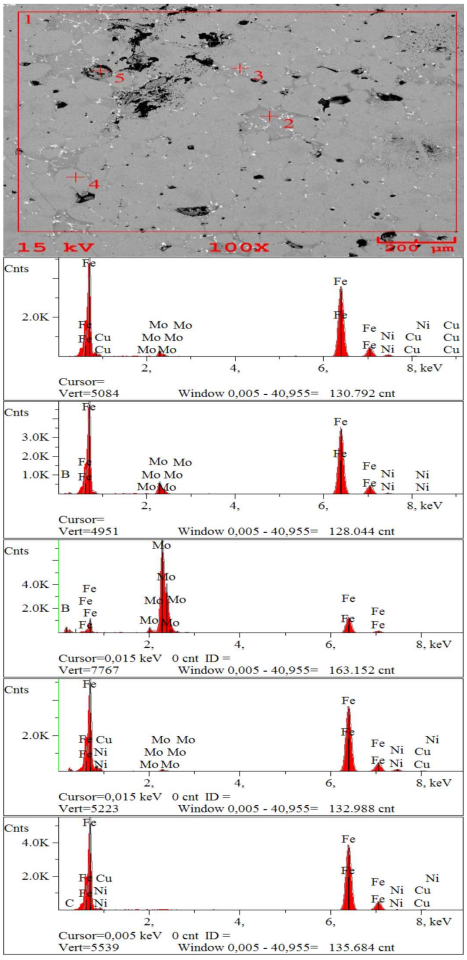

Fig. 6. SEM+EDX analysis of sample sintered at 1250 °C for 90 minutes.

The results of SEM analysis of the studied samples are composed of two different grayscale phases. Probably the dark gray section includes iron-carbon grains. Light-colored matrix grains are including iron-nickel and some copper. White spots are seen to contain Mo element. The main chemical elements were identified as carbon (C), iron (Fe), molybdenum (Mo), copper (Cu) boron (B) and nickel (Ni). The solubility of alloying elements increases in Fe-based alloy with increasing sintering temperature. Figures 4–6 show the EDX results of the samples sintered at temperatures of 1050, 1150 and 1250 °C for sintering time of 90 min.

Figure 7 shows XRD patterns of the specimens after different sintering processes.

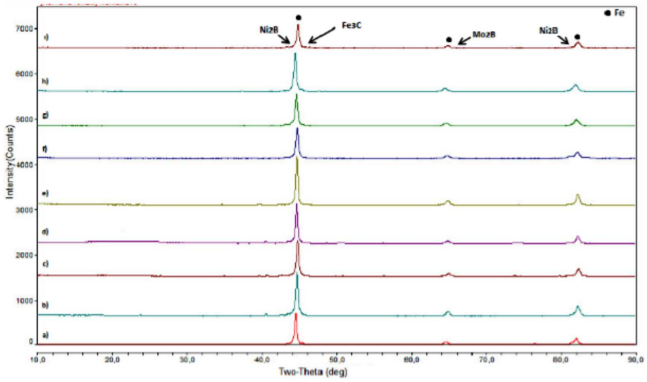

Fig. 7. XRD patterns of samples sintered at 1050 °C for (a) 30 min, (b) 60 min, (c) 90 min; at 1150 °C for (d) 30 min, (e) 60 min, (f) 90 min; at 1250 °C for (g) 30 min, (h) 60 min, (i) 90 min.

As indicated in these spectra, the peaks correspond to iron structure in the samples. It is estimated that the peaks are shifted to the left with the dissolving of the elements in the crystal lattice with increasing sintering temperature and time.

The formation of Fe_3C, Ni_2B, Mo_2B peaks is observed on the edges of iron peaks. Addition of 1% of boron has resulted in creation of new compounds by reaction with nickel and molybdenum. Height of the iron peaks decreases with increasing sintering temperature and time. This is caused by the dissolution of additive elements in iron at high sintering temperature.

4. Conclusions

In this study, the effect of sintering temperature and time on the mechanical properties and microstructure of Fe-0.8C-2.0Cu-4.5Ni-1.8Mo-1.0B metal matrix composite was investigated. The hardness values have increased with increasing sintering temperature and time. The highest hardness value was obtained in samples sintered at 1250 °C for 90 minutes. The highest density value was obtained in sample sintered at 1250 °C for 90 and 60 minutes.

The lowest friction coefficient of 0.23 was obtained in the samples sintered at 1250 °C for 90 minutes. Minimum sample loss of 2.3 mg has also been observed in the same sample. Generally the amount of wear also increases in parallel with the friction coefficient in wear test.

The formation of bainite structure was observed in microstructure with increasing sintering temperature. If the material contains bainitic structure it exhibits low wear rates.

References

[1] J. Wang, H. Danninger, *Wear* **222**, 49 (1998).

[2] A. Simchi, A.A. Nojoomi, *Adv. Powd. Metall.* **2013**, 86 (2013).

[3] K.S. Narasimhan, *Mater. Chem. Phys.* **67**, 56 (2001).

[4] A. Benner, P. Beiss, *Mat.-wiss. u. Werkstofftech.* **35**, 663 (2004).

[5] A. Benner, P. Beiss, *Euro PM2000 Conf. Material and Processing Trends for PM Components in Transportation, Proceedings, Munich*, 2000, p. 101.

[6] E. Robert-Perron, C. Blais, S. Pelletier, Y. Thomas, *Metall. Mater. Trans. A* **38**, 1337 (2007).

[7] E. Robert-Perron, C. Blais, S. Pelletier, Y. Thomas, *Metall. Mater. Trans. A* **38**, 1330 (2007).

[8] L. Tremblay, F. Chagnon, Y. Thomas, M. Gagné, *SAE Technical Paper* **2001**, 2001-01-0399 (2001).

[9] M. Wu, G. Shu, S. Chang, B. Lin, *Metall. Mater. Trans. A* **45**, 3866 (2014).

[10] P. Kumar Bardhan, S. Patra, G. Sutradhar, *Mater. Sci. Applic.* **1**, 152 (2010).

[11] Z.Y. Xiao, M.Y. Ke, L. Fang, M. Shao, Y.Y. Li, *J. Mater. Proc. Technol.* **209**, 4527 (2009).